Supporting Information

Impact of Mutations on the Binding Pocket of Soybean Lipoxygenase: Implications for Proton-Coupled Electron Transfer

Pengfei Li, Alexander V. Soudackov, and Sharon Hammes-Schiffer*

Department of Chemistry, Yale University, 225 Prospect Street, New Haven, Connecticut 06520;
sharon.hammes-schiffer@yale.edu

TABLE OF CONTENTS

Protocol for Binding Pocket Volume Analysis

The POVME2 program[1] was used for the binding pocket volume analysis. The binding pocket cavity (Figure 1A) was obtained by first generating a sphere centered at (20.5, 50.0, 11.0) with a radius of 13 Å. Three contiguous spheres were then placed inside this sphere at (16.0, 49.0, 9.5) with radius 5.0 Å, (20.5, 50.0, 11.0) with radius 5.0 Å, and (25.5, 49.5, 12.5) with radius 5.0 Å. A grid spanning the large sphere was generated with a spacing of 0.5 Å. The points inside the large sphere within 1.09 Å from any protein atom, as well as the points outside the protein's convex hull, were excluded. All other points inside the large sphere were retained if connected to the contiguous spheres using a contiguous point criterion of 1. Finally, the cavity volume was measured as the sum of the retained points, with each point representing a volume of 0.125 $Å^3$. For the volume evaluation of WT SLO and the six mutants shown in Table 2, 20,000 configurations from a 1 μs trajectory for each system were used. The C_α atoms in these configurations were aligned with those in the initial WT SLO structure prior to analysis.

Protocol for Docking

The docking modeling files for WT and DM SLO and linoleic acid were prepared based on Ref 2. The WT and DM SLO structures were obtained from the molecular dynamics equilibration described in Ref. 2, where the cofactor is in the Fe(III)OH state and the substrate is bound, was used for modeling the protein. All protein hydrogen atoms were retained, and the partial charge parameters of the protein were obtained from the Gasteiger charges determined using AutoDockTools.[3] Subsequently, the charges of iron, the hydroxyl oxygen, and the hydroxyl hydrogen were changed to +3, −1 and 0, respectively, to ensure a charge of +2 for the Fe(III)OH group. The partial charges for linoleic acid with the carboxylic acid deprotonated were determined from RESP charges fitting based on the HF/6-31G* level of theory, and all of its hydrogen atoms were retained during docking as well. The Autodock Vina[4] tool was used for the docking procedure. During the docking, the protein was kept fixed, and the two double bonds and two terminal carbon-oxygen bonds of the linoleic acid were fixed while all the other carbon-carbon bonds within linoleic were treated as rotatable. A cubic box centered on the hydroxyl oxygen atom with a side length of 25 Å was used for the docking, and 1998 structures were generated. These structures were filtered according to the following criteria: C-O distance ≤ 3.5 Å, C-Hs-O angle ≥ 120°, and Hs-O-H angle ≥ 100°. Only nine and ten structures satisfied all of these criteria for WT and DM SLO, respectively. Their binding affinities are shown in Tables S1 and S2. For WT SLO, the five structures with the highest binding affinities have similar structures and are classified as carboxylate-in conformations (Figure 1B). The C9-C10 double bond is pinched by the L546 and L754 sidechains in these conformations. A comparison between this docking mode and the substrate binding mode observed in previous QM/MM free energy simulations[2] is provided in Figure S3. A channel analysis for this binding mode using the CAVER Analyst program[5] identified oxygen channels that yield the S configuration of the product (i.e., 13S-hydroperoxyotadecadeinoic acid). These channels are shown in Figure S4. The remaining four structures are classified as carboxylate-out conformations, and the hydrophobic tail occupies an oxygen channel proposed previously (Figures 1A and S2). For DM SLO, five representative structures are illustrated in Figure S5.

Protocol for Molecular Dynamics Simulations

A. Preparation of the initial structures

1. The PDB entries 3PZW, 3BND, 3BNE, 3BNC, 5TQN, 5TR0, and 5TQO were used for modeling the WT, I553V, I553A, I553G, L546A, L754A, and DM SLO, respectively. Chain A of these entries was used if the crystal structure was a dimer. If alternative positions were available for a certain atom, the position with higher occupancy was used except for the HIS499 and HIS504 in the L546A system, for which the conformation B was used because it gives a more reasonable coordination geometry for the metal site.
2. The missing heavy atoms were added for each system using the profix program in the Jakcal software package.[6] Residues that have newly added heavy atom(s) were refined by using the conref program in the Jakcal software package. Water molecules for which the oxygen atom was within 3.0 Å of a heavy atom of these added residues were deleted. Other water molecules were retained for the final modeling.
3. The H++ webserver[7] was used to add protons to the amino acids by setting the salinity as 0.15 M, the internal dielectric constant as 10, the external dielectric as 80, and the pH as 8.0. Subsequently, the protonation states of the metal ligating residues were adjusted if necessary. The protons on the water molecules were added by the tleap program in the AmberTools software package.[8] The metal site was represented in the product state, in which the iron is in the ferrous state (i.e., Fe(II)) and the coordination oxygen is represented by a water molecule, yielding a total charge of +1 and a multiplicity of 5 for the metal site with ligands.

B. Parameterization for the metal center

4. The MCPB.py program[9] was used for the parameterization of the metal center. The WT structure was used for creating the small model and the large model, as defined within this program.[9] The small model was created to obtain the bond force constants between the iron and the ligating atoms, while the large model was used to obtain the partial charge parameters. The torsion barriers of the dihedrals involving the metal ion were treated as zero (i.e., no torsion interaction were considered). The details of the mass, bond, angle, charge, and nonbonded parameters are given in the parameter section of this SI.
5. For the small model, the hydrogen atoms were minimized first, followed by a full optimization. Subsequently, potential energy scans were performed to obtain the force constants between the metal and the ligating atoms. The force constants of the angles involving the metal ion were assigned based on the empirical relationship in the general AMBER force field (GAFF)[10]: (1) if there is one hydrogen atom among the two terminal atoms, the angle force constant was assigned as 50 kcal/(mol•radian^2); (2) if all three atoms are heavy atoms, the angle force constant was assigned as 70 kcal/(mol•radian^2). The equilibrium values of these bonds and angles were obtained from the crystal structures, which were assigned differently for WT and mutant systems, except for the bonds and angles involving hydrogen atoms in the coordinated water molecule because these crystal structures did not include the coordinates of these hydrogen atoms. The equilibrium values of these bonds and angles were determined from the QM optimized structure of the small model. The force constants of the O-H bond and H-O-H angle were obtained from the

quantum calculation of a single water molecule at the B3LYP/6-31G* level of theory using the Seminario method.[11] The force constant of the Fe-O-H angle was obtained from the empirical rule stated above (i.e., as 50 kcal/(mol•radian^2)).

6. The large model was created to obtain the partial charges for the metal site. The van der Waals (VDW) radius of the ferrous ion was obtained from the ion-oxygen distance (IOD) parameter set from Ref 12 for the electrostatic potential (ESP) fitting. The hydrogen atoms were optimized for the large model, and then the RESP fitting algorithm was used for deriving the partial charges. The partial charges of the backbone heavy atoms of the ligating residues were restrained to the corresponding values in the ff14SB force field.[13]

C. Molecular dynamics simulation procedure

7. In addition to the parameters for the metal site, the ff14SB force field was used for modeling the protein system.[13] A cubic water box of the TIP3P water model[14] was used to solvate the system. The minimum distance between the solute and box edge was set as 10 Å. Then Na^+ and Cl^- ions were added to neutralize the system and produce a salt concentration of ~0.15 M for the final production simulations. The VDW parameters of the Na^+ and Cl^- ions were obtained from the hydration free energy (HFE) parameter set for the TIP3P water model.[15] The IOD parameter set for the Fe^{2+} ion[12] was used for the VDW parameters of the ferrous iron in the metal site.
8. At the beginning of the equilibration procedure, minimization, NVT equilibration, and NPT equilibration were performed to minimize and equilibrate the positions of the water molecules, sodium and chloride ions, and hydrogen atoms of the protein. The minimization was performed for 5000 steps with the steepest descent algorithm. The NVT equilibration was performed at 300 K, and the NPT equilibration was performed at 300 K and 1 atmosphere pressure. These steps were performed with a restraint of 500.0 kcal/(mol•Å^2) on the heavy atoms of the protein (except the restraint on the I553G and L754A systems was set as 200.0 kcal/(mol•Å^2) for the NVT and NPT simulations). The Langevin thermostat with a collision frequency of 2 ps^{-1} was used to control the temperature, and the Berendsen barostat with a coupling time of 1.0 ps was used to control the pressure.
9. In the next step of equilibration, a series of minimizations was performed to relax the protein structure: (1) Minimization consisting of 2000 steps with the steepest descent algorithm and 3000 steps with the conjugated gradient algorithm was performed with a restraint of 100.0 kcal/(mol•Å^2) on the heavy atoms of the protein; (2) Minimization consisting of 2000 steps with the steepest descent algorithm followed by 3000 steps with the conjugated gradient algorithm was performed with a restraint of 100.0 kcal/(mol•Å^2) on the backbone C, C_α, and N atoms of the protein; (3) Minimization consisting of 10000 steps with the steepest descent algorithm followed by 10000 steps with the conjugated gradient algorithm was performed with a restraint of 50.0 kcal/(mol•Å^2) on the backbone C, C_α, and N atoms of the protein; (4) Minimization consisting of 2000 steps with the steepest descent algorithm followed by 3000 steps with the conjugated gradient algorithm was performed with a restraint of 10.0 kcal/(mol•Å^2) on the backbone C, C_α, and N atoms of the protein; (5) Full minimization of the system was performed, consisting of 10000 steps with the steepest descent algorithm and 10000 steps with the conjugated gradient algorithm.

10. After the minimization, a heating procedure was performed to gradually heat the system to 300 K, followed by equilibrium molecular dynamics (MD) to further equilibrate the system. The heating and equilibrium MD simulations were conducted in the NPT ensemble. The heating procedure was performed for a total of 360 ps according to the following steps: (1) 10 ps to heat the system from 0 to 50 K, and then 50 ps to equilibrate the system at 50 K; (2) 10 ps to heat the system from 50 K to 100 K, and then 50 ps to equilibrate the system at 100 K; (3) 10 ps to heat the system from 100 K to 150 K, and then 50 ps to equilibrate the system at 150 K; (4) 10 ps to heat the system from 150 K to 200 K, and then 50 ps to equilibrate the system at 200 K; (5) 10 ps to heat the system from 200 K to 250 K, and then 50 ps to equilibrate the system at 250 K; (6) 30 ps to heat the system from 250 K to 300 K, and then 30 ps to equilibrate the system at 300 K. Subsequently, an NPT equilibrium MD trajectory was propagated for 2 ns at 300 K and 1 atmosphere pressure. The Langevin thermostat was used to control the temperature with a collision frequency of 2 ps^{-1} and 1 ps^{-1} for the heating and equilbirum procedures, respectively. The Berendsen barostat was used to control the pressure with a coupling time of 1.0 ps in these simulations.
11. After this comprehensive equilibration procedure, a 1 μs production trajectory was propagated for each protein system. Configurations were stored every 10 ps, yielding 100,000 snapshots for each system. These simulations were carried out in the NVT ensemble at a temperature of 300 K. The Langevin thermostat was used to control the temperature with a collision frequency of 2 ps^{-1}.

For all the minimization and molecular dynamics simulations mentioned in the protocol above, the nonbonded cut off was set as 10 Å, periodic boundary condition (PBC) was used, and the particle mesh Ewald (PME) algorithm[16] was employed to deal with the long-range electrostatic interactions. The SHAKE algorithm[17] was used to constrain the bond distances involving hydrogen atoms except that a "three-point" SHAKE algorithm[18] was used for the solvent water molecules. A 2 fs time-step was used for all of the MD simulations except that a 1 fs time-step was used for the NVT and NPT solvent equilibration, as well as the NPT heating, for the I553G and L754A mutants. The pmemd.MPI or pmemd.cuda program in Amber14[19] was used for the equilibration, while the pmemd.cuda program[20] was used for all of the production simulations.

Force Field Parameters

A. Parameters shared between WT SLO and the mutants

The atom type and charge parameters were the same for the metal site residues in WT SLO and the mutants. These parameters are given below.

1. The atom type and charge parameters for HID499

ATOM NAME	ATOM TYPE	ATOMIC CHARGE	ATOM NAME	ATOM TYPE	ATOMIC CHARGE
N	N	-0.415700	NE2	Y1	-0.094207
CA	CX	0.018800	H	H	0.274212
C	C	0.597300	HA	H1	0.126912
O	O	-0.567900	HB2	HC	0.049981
CB	CT	-0.016015	HB3	HC	0.049981
CG	CC	-0.000190	HD1	H	0.340824
ND1	NA	-0.213472	HD2	H4	0.097036
CD2	CV	-0.141086	HE1	H5	0.174362
CE1	CR	0.008661			

2. The atom type and charge parameters for HID504

ATOM NAME	ATOM TYPE	ATOMIC CHARGE	ATOM NAME	ATOM TYPE	ATOMIC CHARGE
N	N	-0.415700	NE2	Y2	-0.322262
CA	CX	0.018800	H	H	0.353895
C	C	0.597300	HA	H1	0.057918
O	O	-0.567900	HB2	HC	0.020375
CB	CT	-0.043296	HB3	HC	0.020375
CG	CC	0.078396	HD1	H	0.304596
ND1	NA	-0.134471	HD2	H4	0.156644
CD2	CV	-0.131294	HE1	H5	0.153902
CE1	CR	0.011384			

3. The atom type and charge parameters for HID690

ATOM NAME	ATOM TYPE	ATOMIC CHARGE	ATOM NAME	ATOM TYPE	ATOMIC CHARGE
N	N	-0.415700	NE2	Y3	-0.110786
CA	CX	0.018800	H	H	0.304073
C	C	0.597300	HA	H1	0.131011
O	O	-0.567900	HB2	HC	0.067564
CB	CT	-0.062986	HB3	HC	0.067564
CG	CC	0.047263	HD1	H	0.288714
ND1	NA	-0.134611	HD2	H4	0.222487
CD2	CV	-0.295279	HE1	H5	0.163724
CE1	CR	0.016261			

4. The atom type and charge parameters for ASN694

ATOM NAME	ATOM TYPE	ATOMIC CHARGE	ATOM NAME	ATOM TYPE	ATOMIC CHARGE
N	N	-0.415700	ND2	N	-0.656770
CA	CX	0.014300	H	H	0.294225
C	C	0.597300	HA	H1	0.085216
O	O	-0.567900	HB2	HC	-0.017506
CB	2C	0.108166	HB3	HC	-0.017506
CG	C	0.353526	HD21	H	0.372554
OD1	Y4	-0.408006	HD22	H	0.313416

5. The atom type and charge parameters for ILE839

ATOM NAME	ATOM TYPE	ATOMIC CHARGE	ATOM NAME	ATOM TYPE	ATOMIC CHARGE
N	N	-0.426700	HA	H1	0.102913
CA	CX	0.008755	HB	HC	0.068350
C	C	0.537019	HG12	HC	0.035855
O	O2	-0.557006	HG13	HC	0.035855
CB	3C	0.096784	HG21	HC	0.042586
CG1	2C	-0.057700	HG22	HC	0.042586
CG2	CT	-0.239396	HG23	HC	0.042586
CD1	CT	-0.108216	HD11	HC	0.031929
OXT	Y5	-0.483647	HD12	HC	0.031929
H	H	0.186105	HD13	HC	0.031929

6. The atom type and charge parameters for ferrous iron

ATOM NAME	ATOM TYPE	ATOMIC CHARGE
FE	M1	0.687848

7. The atom type and charge parameters for the coordinated water molecule

ATOM NAME	ATOM TYPE	ATOMIC CHARGE
O	Y6	-0.797832
H1	HX	0.437355
H2	HY	0.409137

The mass and nonbonded parameters of the metal site, along with the bond and angle parameters of the metal site water molecule, were the same for WT SLO and the mutants. These parameters are given below.

```
MASS
M1 55.85                    Fe ion
Y1 14.01      0.530         sp2 N in 5 memb.ring w/LP (HIS,ADE,GUA)
Y2 14.01      0.530         sp2 N in 5 memb.ring w/LP (HIS,ADE,GUA)
Y3 14.01      0.530         sp2 N in 5 memb.ring w/LP (HIS,ADE,GUA)
Y4 16.00      0.434         carbonyl group oxygen
Y5 16.00      0.434         carboxyl and phosphate group oxygen
Y6 16.00      0.000         oxygen in TIP3P water
HX 1.008      0.000         H1 in TIP3P water (coordinating to the carboxyl oxygen)
HY 1.008      0.000         H2 in TIP3P water

BOND
Y6-HX  562.5   1.0113    ADD BY PENGFEI BASED ON Seminario method at B3LYP/6-31G* level of theory
Y6-HY  562.5   0.9682    ADD BY PENGFEI BASED ON Seminario method at B3LYP/6-31G* level of theory

ANGL
HX-Y6-HY   49.51    108.74   ADD BY PENGFEI BASED ON Seminario method at B3LYP/6-31G* level of theory

NONB
 M1       1.4090  0.0172100000      IOD set for Fe2+ ion from Li et al. JCTC, 2013, 9, 2733
 Y1       1.8240  0.1700            OPLS
 Y2       1.8240  0.1700            OPLS
 Y3       1.8240  0.1700            OPLS
 Y4       1.6612  0.2100            OPLS
 Y5       1.6612  0.2100            OPLS
 Y6       1.7683  0.1520            TIP3P water model
 HX       0.0     0.0
 HY       0.0     0.0
```

B. Parameters that are different in WT SLO and the mutants

In terms of the force field parameters associated with the metal ion involving bond and angles, the force constants were the same for all of the systems studied, but the equilibrium values were obtained from the corresponding crystal structure of each species. These parameters are given below.

1. WT

BOND

M1-Y6	138.6	2.1120
Y1-M1	123.7	2.2370
Y2-M1	113.5	2.3480
Y3-M1	131.5	2.2660
Y4-M1	102.2	2.8480
Y5-M1	194.0	2.2380

ANGL

C -Y4-M1	70.00	119.63
C -Y5-M1	70.00	131.96
CR-Y1-M1	70.00	117.91
CR-Y2-M1	70.00	119.26
CR-Y3-M1	70.00	129.45
CV-Y1-M1	70.00	131.57
CV-Y2-M1	70.00	131.25
CV-Y3-M1	70.00	124.04
M1-Y6-HX	50.00	102.45
M1-Y6-HY	50.00	121.64
Y1-M1-Y2	70.00	95.21
Y1-M1-Y3	70.00	100.45
Y1-M1-Y4	70.00	73.34
Y1-M1-Y5	70.00	166.73
Y1-M1-Y6	70.00	86.98
Y2-M1-Y3	70.00	102.17
Y2-M1-Y4	70.00	163.85
Y2-M1-Y5	70.00	95.40
Y2-M1-Y6	70.00	96.86
Y3-M1-Y4	70.00	91.28
Y3-M1-Y5	70.00	85.06
Y3-M1-Y6	70.00	158.77
Y4-M1-Y5	70.00	94.62
Y4-M1-Y6	70.00	71.67
Y5-M1-Y6	70.00	83.86

2. I553V

BOND

M1-Y6	138.6	2.1400
Y1-M1	123.7	2.1650
Y2-M1	113.5	2.3000
Y3-M1	131.5	2.1960
Y4-M1	102.2	2.5060
Y5-M1	194.0	2.2370

ANGL

C -Y4-M1	70.00	132.28
C -Y5-M1	70.00	131.13
CR-Y1-M1	70.00	113.64
CR-Y2-M1	70.00	119.68
CR-Y3-M1	70.00	123.48
CV-Y1-M1	70.00	136.59
CV-Y2-M1	70.00	131.50
CV-Y3-M1	70.00	127.31
M1-Y6-HX	50.00	102.45
M1-Y6-HY	50.00	121.64
Y1-M1-Y2	70.00	91.97
Y1-M1-Y3	70.00	99.69
Y1-M1-Y4	70.00	81.85
Y1-M1-Y5	70.00	171.66
Y1-M1-Y6	70.00	86.91
Y2-M1-Y3	70.00	98.25
Y2-M1-Y4	70.00	169.70
Y2-M1-Y5	70.00	92.24
Y2-M1-Y6	70.00	91.92
Y3-M1-Y4	70.00	90.93
Y3-M1-Y5	70.00	86.82
Y3-M1-Y6	70.00	167.63
Y4-M1-Y5	70.00	92.92
Y4-M1-Y6	70.00	79.58
Y5-M1-Y6	70.00	85.75

3. I553A

BOND
M1-Y6 138.6 2.1600
Y1-M1 123.7 2.1850
Y2-M1 113.5 2.3020
Y3-M1 131.5 2.1790
Y4-M1 102.2 2.4100
Y5-M1 194.0 2.1960

ANGL
C -Y4-M1 70.00 132.71
C -Y5-M1 70.00 131.26
CR-Y1-M1 70.00 116.81
CR-Y2-M1 70.00 120.55
CR-Y3-M1 70.00 125.76
CV-Y1-M1 70.00 134.34
CV-Y2-M1 70.00 130.72
CV-Y3-M1 70.00 126.22
M1-Y6-HX 50.00 102.45
M1-Y6-HY 50.00 121.64
Y1-M1-Y2 70.00 92.28
Y1-M1-Y3 70.00 101.85
Y1-M1-Y4 70.00 83.15
Y1-M1-Y5 70.00 170.28
Y1-M1-Y6 70.00 84.99
Y2-M1-Y3 70.00 98.98
Y2-M1-Y4 70.00 169.02
Y2-M1-Y5 70.00 92.60
Y2-M1-Y6 70.00 91.28
Y3-M1-Y4 70.00 91.75
Y3-M1-Y5 70.00 85.67
Y3-M1-Y6 70.00 167.36
Y4-M1-Y5 70.00 90.54
Y4-M1-Y6 70.00 78.40
Y5-M1-Y6 70.00 86.51

4. I553G

BOND
M1-Y6 138.6 2.1640
Y1-M1 123.7 2.2350
Y2-M1 113.5 2.2270
Y3-M1 131.5 2.1880
Y4-M1 102.2 2.7920
Y5-M1 194.0 2.2410

ANGL
C -Y4-M1 70.00 123.35
C -Y5-M1 70.00 130.54
CR-Y1-M1 70.00 114.67
CR-Y2-M1 70.00 115.03
CR-Y3-M1 70.00 126.50
CV-Y1-M1 70.00 135.47
CV-Y2-M1 70.00 135.37
CV-Y3-M1 70.00 124.65
M1-Y6-HX 50.00 102.45
M1-Y6-HY 50.00 121.64
Y1-M1-Y2 70.00 90.04
Y1-M1-Y3 70.00 101.07
Y1-M1-Y4 70.00 77.97
Y1-M1-Y5 70.00 168.74
Y1-M1-Y6 70.00 83.33
Y2-M1-Y3 70.00 101.72
Y2-M1-Y4 70.00 164.59
Y2-M1-Y5 70.00 98.75
Y2-M1-Y6 70.00 98.46
Y3-M1-Y4 70.00 90.17
Y3-M1-Y5 70.00 84.11
Y3-M1-Y6 70.00 159.31
Y4-M1-Y5 70.00 92.12
Y4-M1-Y6 70.00 70.82
Y5-M1-Y6 70.00 88.39

5. L546A

BOND
M1-Y6 138.6 2.3010
Y1-M1 123.7 2.3830
Y2-M1 113.5 2.3600
Y3-M1 131.5 2.3270
Y4-M1 102.2 3.3090
Y5-M1 194.0 2.3160

ANGL
C -Y4-M1 70.00 104.59
C -Y5-M1 70.00 129.61

CR-Y1-M1 70.00 127.13
CR-Y2-M1 70.00 142.09
CR-Y3-M1 70.00 129.58
CV-Y1-M1 70.00 121.98
CV-Y2-M1 70.00 107.33
CV-Y3-M1 70.00 121.16
M1-Y6-HX 50.00 102.45
M1-Y6-HY 50.00 121.64
Y1-M1-Y2 70.00 92.31
Y1-M1-Y3 70.00 115.44
Y1-M1-Y4 70.00 82.60
Y1-M1-Y5 70.00 158.64
Y1-M1-Y6 70.00 76.34
Y2-M1-Y3 70.00 101.11
Y2-M1-Y4 70.00 169.81
Y2-M1-Y5 70.00 83.36
Y2-M1-Y6 70.00 103.46
Y3-M1-Y4 70.00 89.06
Y3-M1-Y5 70.00 85.92
Y3-M1-Y6 70.00 152.25
Y4-M1-Y5 70.00 98.17
Y4-M1-Y6 70.00 66.80
Y5-M1-Y6 70.00 84.31

6. L754A

BOND
M1-Y6 138.6 2.1240
Y1-M1 123.7 2.4640
Y2-M1 113.5 2.3430
Y3-M1 131.5 2.4080
Y4-M1 102.2 3.2480
Y5-M1 194.0 2.3020

ANGL
C -Y4-M1 70.00 103.57
C -Y5-M1 70.00 123.89
CR-Y1-M1 70.00 142.32
CR-Y2-M1 70.00 129.05
CR-Y3-M1 70.00 136.53
CV-Y1-M1 70.00 108.44
CV-Y2-M1 70.00 120.42
CV-Y3-M1 70.00 114.42
M1-Y6-HX 50.00 102.45
M1-Y6-HY 50.00 121.64
Y1-M1-Y2 70.00 79.11
Y1-M1-Y3 70.00 125.21
Y1-M1-Y4 70.00 82.56
Y1-M1-Y5 70.00 153.30
Y1-M1-Y6 70.00 65.65
Y2-M1-Y3 70.00 110.67
Y2-M1-Y4 70.00 159.12
Y2-M1-Y5 70.00 89.65
Y2-M1-Y6 70.00 81.35
Y3-M1-Y4 70.00 88.09
Y3-M1-Y5 70.00 81.38
Y3-M1-Y6 70.00 164.34
Y4-M1-Y5 70.00 102.60
Y4-M1-Y6 70.00 82.05
Y5-M1-Y6 70.00 88.89

7. DM

BOND
M1-Y6 138.6 2.0980
Y1-M1 123.7 2.2730
Y2-M1 113.5 2.2580
Y3-M1 131.5 2.2960
Y4-M1 102.2 3.5000
Y5-M1 194.0 2.2820

ANGL
C -Y4-M1 70.00 93.64
C -Y5-M1 70.00 135.80
CR-Y1-M1 70.00 120.45
CR-Y2-M1 70.00 128.66
CR-Y3-M1 70.00 129.90
CV-Y1-M1 70.00 130.44
CV-Y2-M1 70.00 121.94
CV-Y3-M1 70.00 121.07
M1-Y6-HX 50.00 102.45
M1-Y6-HY 50.00 121.64
Y1-M1-Y2 70.00 86.47
Y1-M1-Y3 70.00 108.10
Y1-M1-Y4 70.00 78.02
Y1-M1-Y5 70.00 160.47
Y1-M1-Y6 70.00 78.45
Y2-M1-Y3 70.00 107.99
Y2-M1-Y4 70.00 160.19

Y2-M1-Y5	70.00	89.65
Y2-M1-Y6	70.00	101.41
Y3-M1-Y4	70.00	88.69
Y3-M1-Y5	70.00	91.31
Y3-M1-Y6	70.00	150.13
Y4-M1-Y5	70.00	100.85
Y4-M1-Y6	70.00	63.67
Y5-M1-Y6	70.00	83.59

Figures

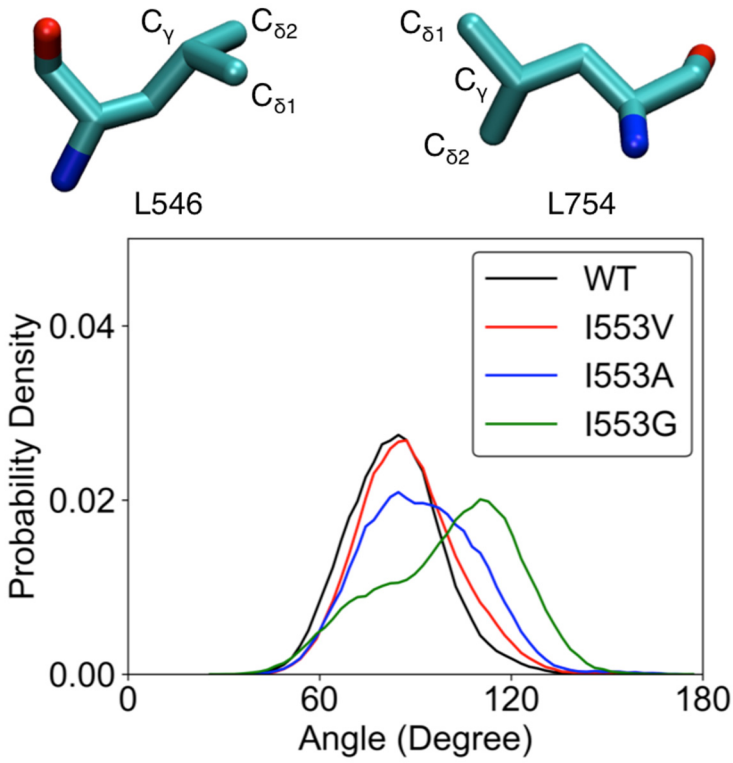

Figure S1. The probability distribution for the angle between the plane containing the C_{γ}, $C_{\delta 1}$, and $C_{\delta 2}$ atoms in the L546 sidechain and the corresponding plane of the L754 sidechain for the WT, I553V, I553A, and I553G SLO systems. The average angles for the WT, I553V, I553A, and I553G SLO systems are 84°, 88°, 92°, and 100°, respectively.

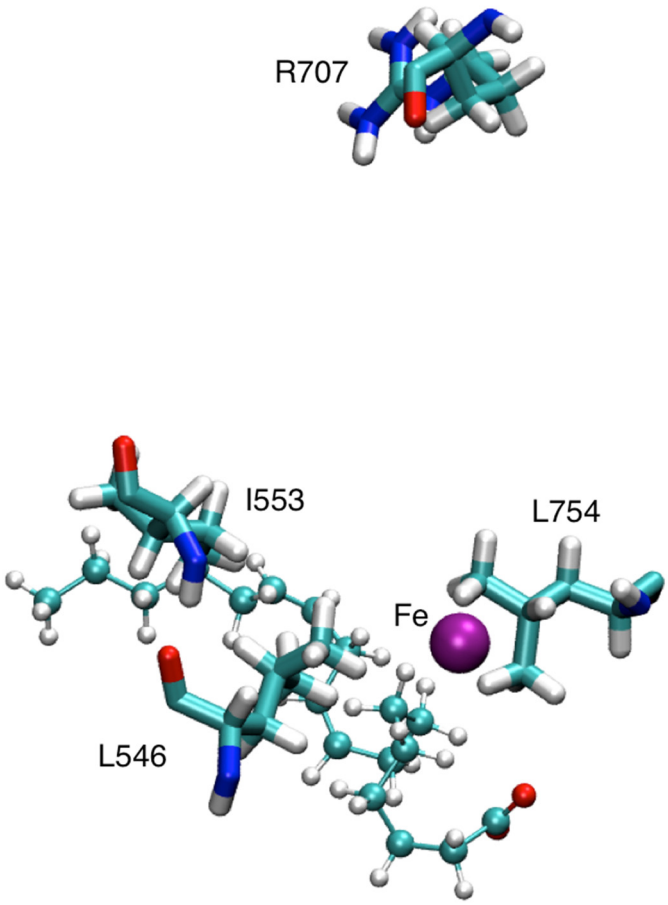

Figure S2. Depiction of a representative carboxylate-out docking mode for WT SLO. This docking mode is one of two modes with the highest affinity among the four carboxylate-out docking modes that satisfy the geometric critiera.

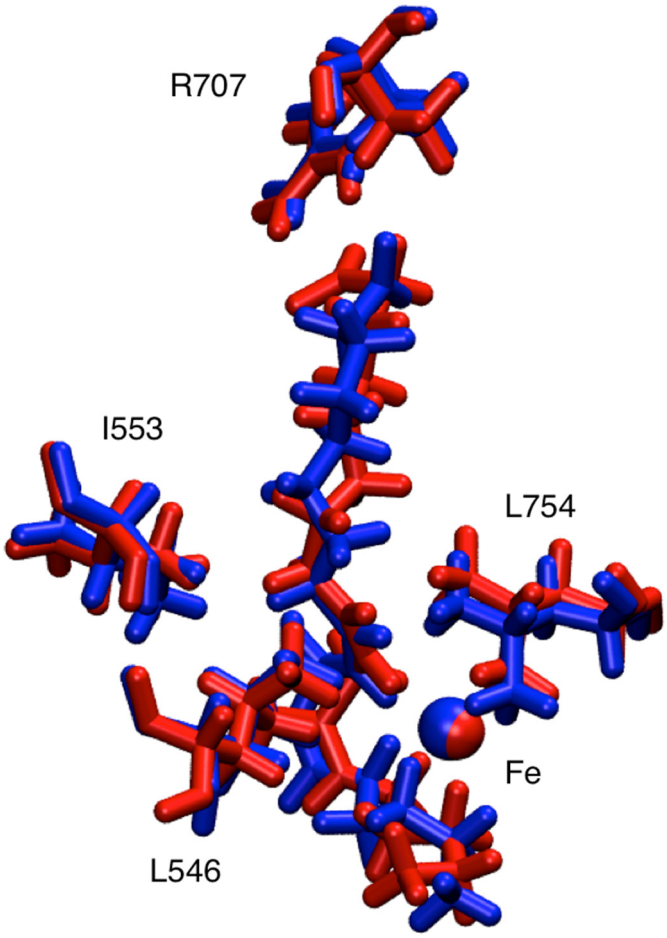

Figure S3. Comparison between the docking mode with the highest affinity among the five carboxylate-in conformations obtained with AutoDock and the substrate binding mode observed in QM/MM free energy simulations with restraints applied to the proton transfer interface.[2] The docking mode is shown in blue, while the substrate binding mode from the QM/MM free energy simulations is shown in red. These substrate binding modes are qualitatively similar.

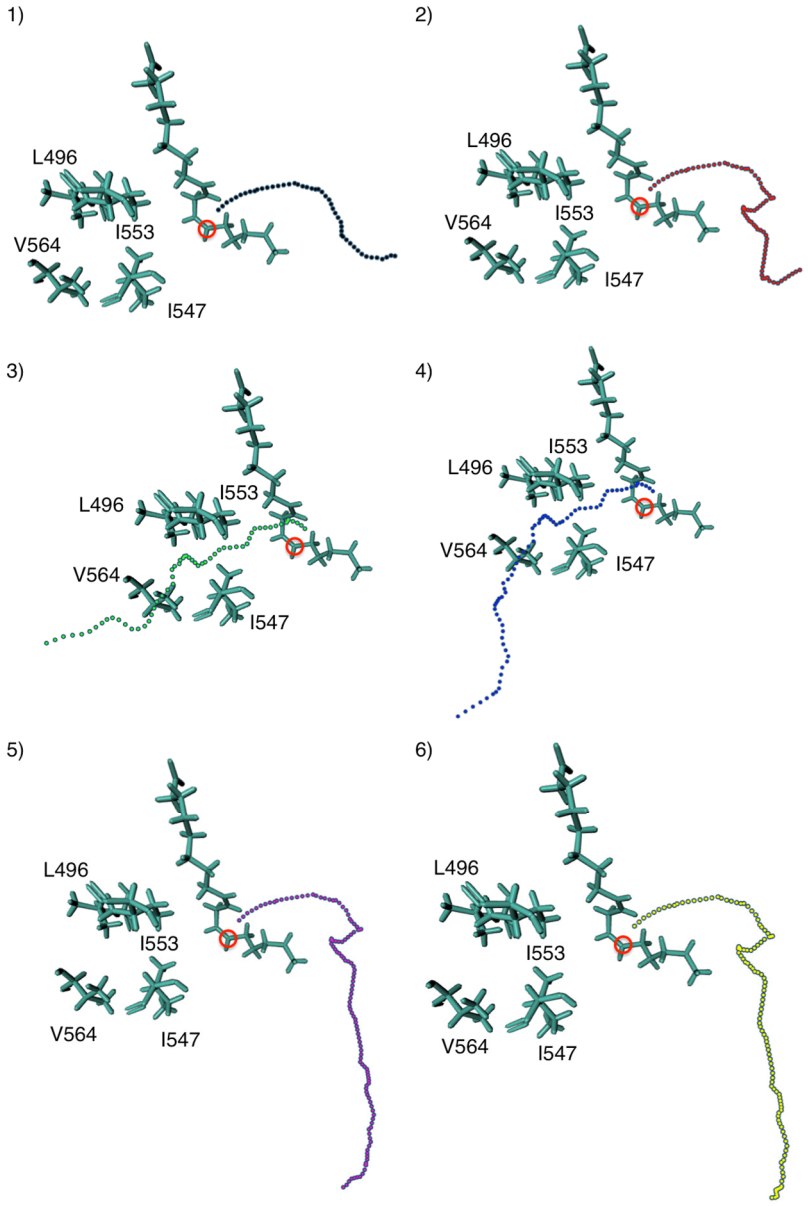

Figure S4. Depiction of the substrate binding mode of linoleic acid to WT SLO identified through the docking procedure to have the highest affinity among the configurations that satisfy the geometry criteria designed to select conformations suitable for PCET, along with the six possible oxygen channels identified by the CAVER Analyst program[5] for this docked conformation. Note that the channel pairs 1 and 2, 3 and 4, and 5 and 6 are very similar. The C13 atom was treated as the starting point for the analysis and is indicated by a red circle. All of these channels would enable the oxygen to attack the C13 atom in a manner that would generate the correct stereoconfiguration of the product. Channels 3 and 4 are consistent with a channel proposed in previous research[21] and is shown in Figure 1A.

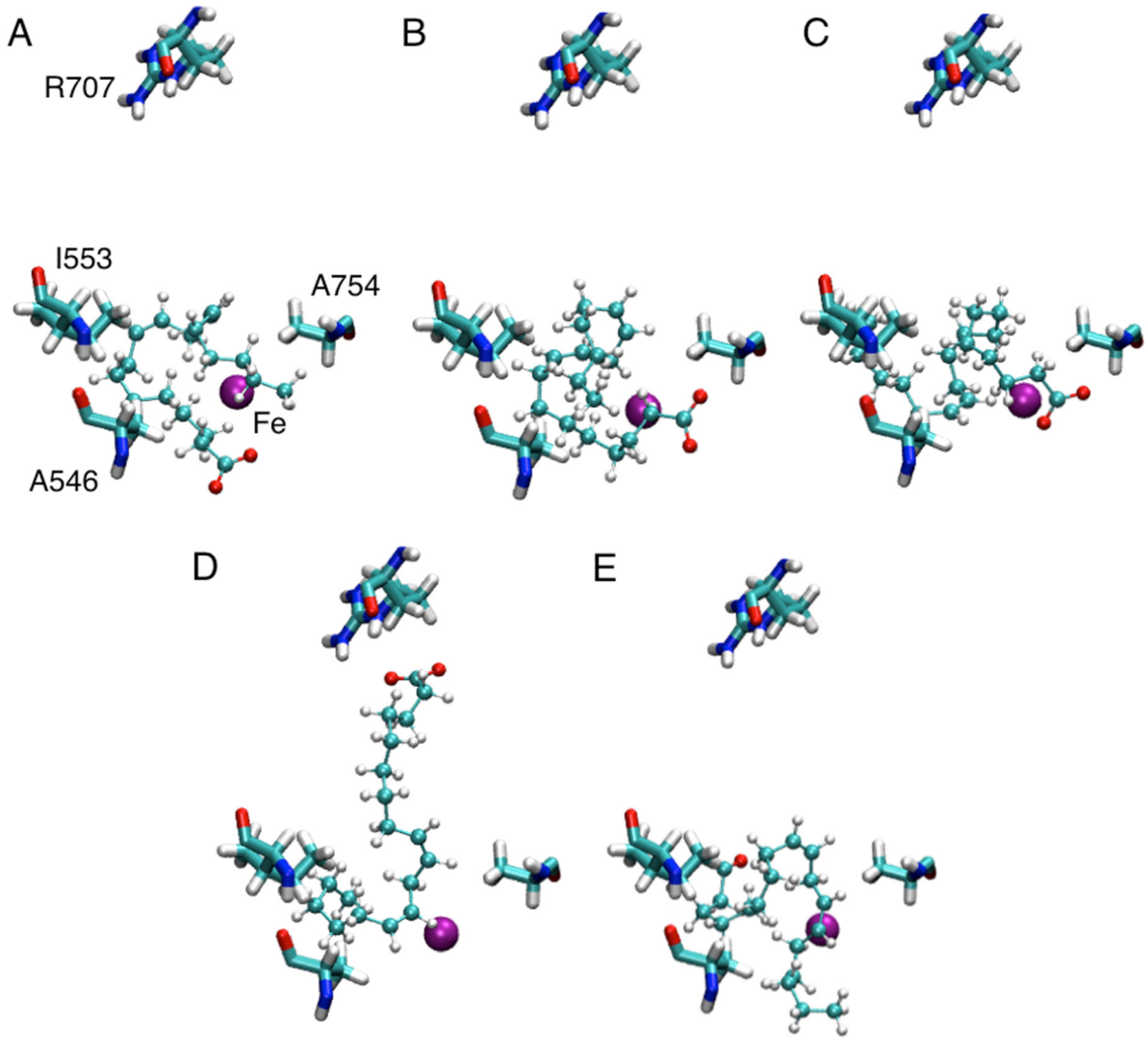

Figure S5. Five representative structures for the docking modes of DM SLO that satisfy the geometric criteria. The larger binding cavity enables the substrate to adopt a wider range of conformations. In the previous QM/MM free energy simulations,[2] the initial substrate binding mode was chosen to be similar to the WT substrate binding mode using a rigid substrate to enable a consistent comparison between the WT and DM free energy surfaces. The substrate binding mode from the previous QM/MM free energy simulations of the DM is qualitatively similar to that shown in (D).

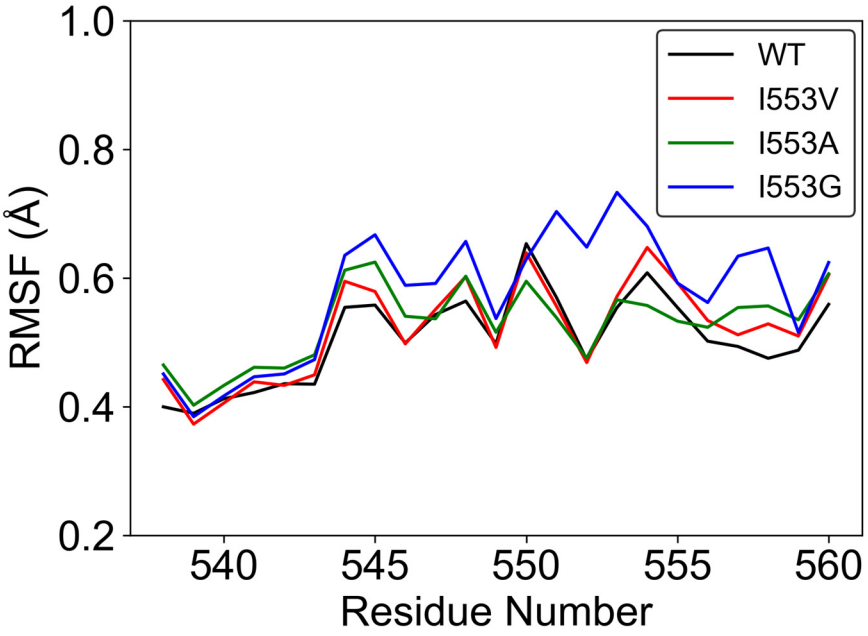

Figure S6. RMSF values of the C_α atoms in residues 538-560 for the WT, I553V, I553A, and I553G SLO systems.

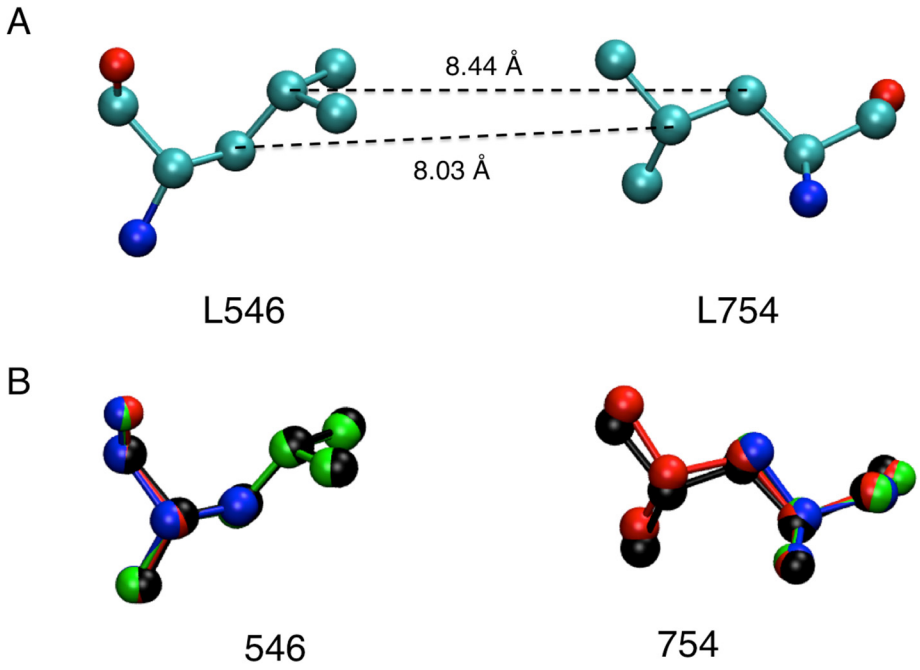

Figure S7. (A) Depiction of the asymmetric orientation of L546 and L754 in the WT SLO system: the distance between C_β of L546 to C_γ of L754 is 8.03 Å, while the distance between C_γ of L546 and C_β of L754 is 8.44 Å. (B) Alignment of the structures of WT, L546A, L754A, and DM systems (black: WT, red: L546A, green: L754A, blue: DM). These structures exhibit the highest occupancy in chain A of PDB entries 3PZW, 5TQN, 5TR0, and 5TQO, respectively. The alignment was performed by aligning the backbone heavy atoms of residues 546 and 754, illustrating only minor differences in the orientations of residues 546 and 754 among these systems. Mutation of Leu to Ala does not significantly alter the relative positions of the C_β atoms in these two residues. The asymmetric orientation shown in (A) is consistent with the larger average distance observed between the sidechains of residues 546 and 754 for L546A compared to L754A, as shown in Figure 3.

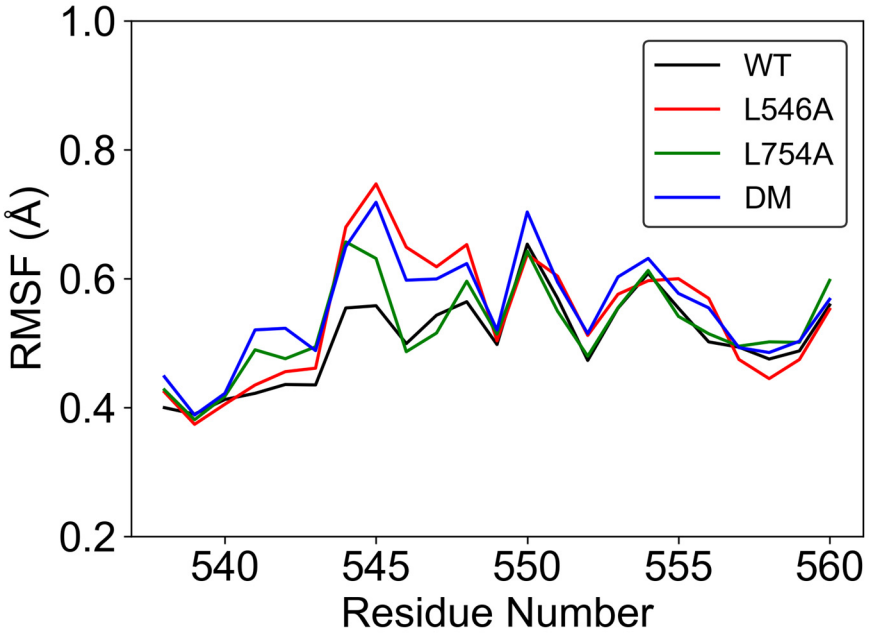

Figure S8. RMSF values of the C_α atoms in residues 538-560 for the WT, L546A, L754A, and DM SLO systems.

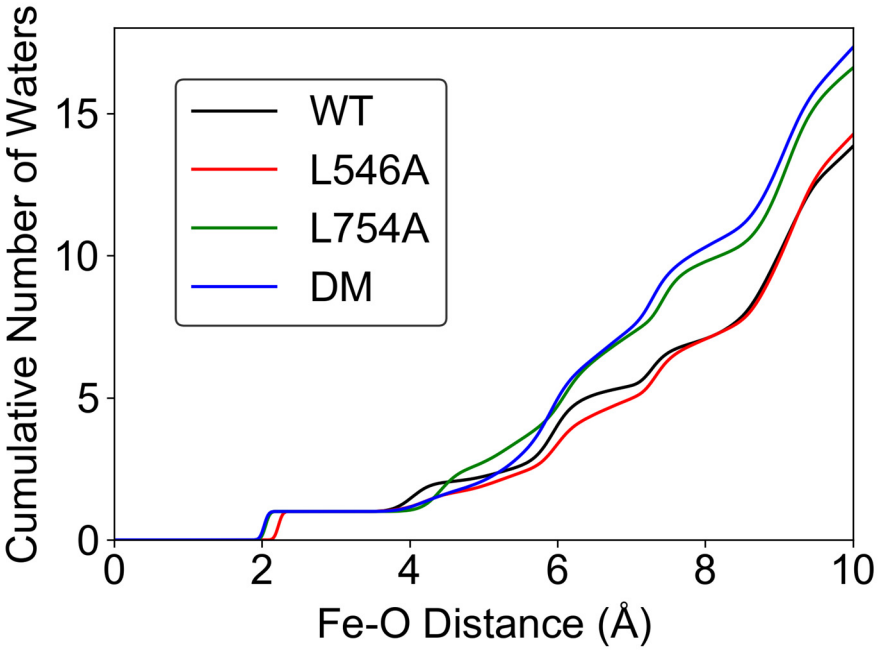

Figure S9. The cumulative number of water oxygen atoms within 10 Å of the iron in the microsecond MD trajectories of the WT, L546A, L754A, and DM SLO systems.

Tables

Table S1. Binding Affinities of the Nine Structures for WT SLO that Satisfy the Criteria Designed to Select Conformations Suitable for PCET[a]

Rank	Binding Affinity (kcal/mol)
1	-4.4
2	-4.3
3	-4.1
4	-4.0
5	-3.5
6/7	-2.6
8	-2.4
9	-1.7

[a]The five structures with the highest affinities are in the carboxylate-in conformation, while the other four are in the carboxylate-out conformation.

Table S2. Binding Affinities of the Ten Structures for DM SLO that Satisfy the Criteria Designed to Select Conformations Suitable for PCET

Rank	Binding Affinity (kcal/mol)
1	-5.9
2	-5.7
3	-5.5
4	-5.4
5	-5.2
6/7	-5.0
8	-4.8
9	-4.8
10	-4.7

References

1. Durrant, J. D.; Votapka, L.; Sørensen, J.; Amaro, R. E., POVME 2.0: an enhanced tool for determining pocket shape and volume characteristics. *J. Chem. Theory Comput.* **2014,** *10*, 5047-5056.
2. Li, P.; Soudackov, A. V.; Hammes-Schiffer, S., Fundamental Insights into Proton-Coupled Electron Transfer in Soybean Lipoxygenase from Quantum Mechanical/Molecular Mechanical Free Energy Simulations. *J. Am. Chem. Soc.* **2018,** *140*, 3068-3076.
3. Morris, G. M.; Huey, R.; Lindstrom, W.; Sanner, M. F.; Belew, R. K.; Goodsell, D. S.; Olson, A. J., AutoDock4 and AutoDockTools4: Automated docking with selective receptor flexibility. *J. Comput. Chem.* **2009,** *30*, 2785-2791.
4. Trott, O.; Olson, A. J., AutoDock Vina: improving the speed and accuracy of docking with a new scoring function, efficient optimization, and multithreading. *J. Comput. Chem.* **2010,** *31*, 455-461.
5. Kozlikova, B.; Sebestova, E.; Sustr, V.; Brezovsky, J.; Strnad, O.; Daniel, L.; Bednar, D.; Pavelka, A.; Manak, M.; Bezdeka, M., CAVER Analyst 1.0: graphic tool for interactive visualization and analysis of tunnels and channels in protein structures. *Bioinformatics* **2014,** *30*, 2684-2685.
6. Xiang, Z.; Honig, B., Extending the accuracy limits of prediction for side-chain conformations. *J. Mol. Biol.* **2001,** *311*, 421-430.
7. Gordon, J. C.; Myers, J. B.; Folta, T.; Shoja, V.; Heath, L. S.; Onufriev, A., H++: a server for estimating pKas and adding missing hydrogens to macromolecules. *Nucleic Acids Res.* **2005,** *33*, W368-W371.
8. Case, D. A.; Cheatham, T. E.; Darden, T.; Gohlke, H.; Luo, R.; Merz Jr, K. M.; Onufriev, A.; Simmerling, C.; Wang, B.; Woods, R. J., The Amber biomolecular simulation programs. *J. Comput. Chem.* **2005,** *26*, 1668-1688.
9. Li, P.; Merz Jr, K. M., MCPB.py: A Python Based Metal Center Parameter Builder. *J. Chem. Inf. Model.* **2016,** *56*, 599-604.
10. Wang, J.; Wolf, R. M.; Caldwell, J. W.; Kollman, P. A.; Case, D. A., Development and testing of a general amber force field. *J. Comput. Chem.* **2004,** *25*, 1157-1174.
11. Seminario, J. M., Calculation of intramolecular force fields from second ‐ derivative tensors. *Int. J. Quantum Chem* **1996,** *60*, 1271-1277.
12. Li, P.; Roberts, B. P.; Chakravorty, D. K.; Merz Jr, K. M., Rational Design of Particle Mesh Ewald Compatible Lennard-Jones Parameters for +2 Metal Cations in Explicit Solvent. *J. Chem. Theory Comput.* **2013,** *9*, 2733-2748.
13. Maier, J. A.; Martinez, C.; Kasavajhala, K.; Wickstrom, L.; Hauser, K. E.; Simmerling, C., ff14SB: improving the accuracy of protein side chain and backbone parameters from ff99SB. *J. Chem. Theory Comput.* **2015,** *11*, 3696-3713.
14. Jorgensen, W. L.; Chandrasekhar, J.; Madura, J. D.; Impey, R. W.; Klein, M. L., Comparison of simple potential functions for simulating liquid water. *J. Chem. Phys.* **1983,** *79*, 926-935.
15. Li, P.; Song, L. F.; Merz Jr, K. M., Systematic Parameterization of Monovalent Ions Employing the Nonbonded Model. *J. Chem. Theory Comput.* **2015,** *11*, 1645-1657.

16. Darden, T.; York, D.; Pedersen, L., Particle mesh Ewald: An N□log(N) method for Ewald sums in large systems. *J. Chem. Phys.* **1993,** *98*, 10089-10092.
17. Ryckaert, J.-P.; Ciccotti, G.; Berendsen, H. J., Numerical integration of the cartesian equations of motion of a system with constraints: molecular dynamics of n-alkanes. *J. Comput. Phys.* **1977,** *23*, 327-341.
18. Miyamoto, S.; Kollman, P. A., SETTLE: an analytical version of the SHAKE and RATTLE algorithm for rigid water models. *J. Comput. Chem.* **1992,** *13*, 952-962.
19. Case, D. A.; Babin, V.; Berryman, J. T.; Betz, R. M.; Cai, Q.; Cerutti, D. S.; Cheatham III, T. E.; Darden, T. A.; Duke, R. E.; Gohlke, H.; Goetz, A. W.; Gusarov, S.; Homeyer, N.; Janowski, P.; Kaus, J.; Kolossváry, I.; Kovalenko, A.; Lee, T. S.; LeGrand, S.; Luchko, T.; Luo, R.; Madej, B.; Merz Jr, K. M.; Paesani, F.; Roe, D. R.; Roitberg, A.; Sagui, C.; Salomon-Ferrer, R.; Seabra, G.; Simmerling, C. L.; Smith, W.; Swails, J.; Walker, R. C.; Wang, J.; Wolf, R. M.; Wu, X.; Kollman, P. A. *AMBER 14*, University of California, San Francisco: 2014.
20. Salomon-Ferrer, R.; Götz, A. W.; Poole, D.; Le Grand, S.; Walker, R. C., Routine Microsecond Molecular Dynamics Simulations with AMBER on GPUs. 2. Explicit Solvent Particle Mesh Ewald. *J. Chem. Theory Comput.* **2013,** *9*, 3878-3888.
21. Collazo, L.; Klinman, J. P., Control of the Position of Oxygen Delivery in Soybean Lipoxygenase-1 by Amino Acid Side Chains within a Gas Migration Channel. *J. Biol. Chem.* **2016,** *291*, 9052-9059.